International Journal of Computational Methods
Vol. 16, No. 6 (2019) 1840022 (18 pages)

DOI: 10.1142/S0219876218400224

Numerical Study on Ship Motion Fully Coupled with LNG Tank Sloshing in CFD Method

Yuan Zhuang and Decheng Wan*

State Key Laboratory of Ocean Engineering
School of Naval Architecture, Ocean and Civil Engineering
Shanghai Jiao Tong University
Collaborative Innovation Center for Advanced Ship and Deep-Sea Exploration
Shanghai 200240, P. R. China
**dcwan@sjtu.edu.cn*

Received 20 December 2016
Accepted 26 October 2017
Published 19 December 2017

In this paper, numerical simulations of ship motion coupled with LNG tank sloshing in waves are considered. The fully coupled problems are performed by our in-house RANS/DES solver, naoe-FOAM-SJTU. The internal tank sloshing and external wave flow are solved simultaneously. The considered model is a three-dimensional simplified LNG FPSO with two prismatic tanks. The ship motion responses are carried out in beam waves to compare with existing experimental data to validate this solver. The coupling effects between ship motion and sloshing tanks are observed. The anti-rolling characteristics are found, and this kind of characteristic is obvious in low-filling conditions. Different incident wave amplitudes and frequencies are considered. When the incident wave frequency is close to ship motion natural frequency, the ship motion response is strong and an overturning behavior in sloshing tanks is observed. Meanwhile, impact pressures on bulkhead are also discussed. The pressure signal explains the phenomenon in tanks we discussed before.

Keywords: LNG FPSO; sloshing; coupling effect; naoe-FOAM-SJTU solver.

1. Introduction

With the development of offshore engineering and the demand for clean energy, the transportation and storage of liquefied natural gas (LNG) have become more essential. Therefore, the needs for ships coupled with LNG tanks such as FPSO and FLNG are attracted more attention. The performance of ship motion coupled with partially filled tanks is different from that without tanks. The ship motion with tanks is affected both by external wave excitation and internal flow. That is, ship motion generates tank sloshing while the sloshing-induced forces and moments will influence ship motion in return. This kind of coupling effect is critical for tank

*Corresponding author.

structural design. Violent sloshing flow in tanks may cause large deformation and impulsive pressure on internal structure, particularly when the external wave frequency is close to that of ship motion coupled with partially filled tanks. The impact loading is sensitive to the excitation of sloshing, which is the ship motion, thus it's important to analyze the impact loading on tanks. For ship motion, the prediction and description of its dynamic characteristics can be complex due to the coupling effect. A good example is the application of anti-rolling tanks (ARTs), which reduce the roll motion of the ship. Another example of the coupling effect is the instability of ship motion caused by deck sloshing. Therefore, it's essential to study the coupling effect of ship motion with partially filled tanks.

Several researches about sloshing tanks have been done in early times, before the effect of sloshing tanks on ship motion was considered. Mikelis *et al.* [1984] used a two-dimensional finite difference transient solution to solve liquid cargo sloshing motions and pressures. Some initial computations have been done on coupled problems of sloshing and ship motion to compare with the experiments. Rognebakke and Faltinsen [2003] conducted two-dimensional experiments of a hull section containing tanks filled with water excited by regular waves, and conducted simulated modeled case using linear and nonlinear sloshing models and, assuming external flow linear. Malenica *et al.* [2003] considered the coupling effect under classical assumptions of linear potential theory and Boundary Integral Equations method. In those researches, tank dynamics are analyzed separately from the exterior radiation and diraction problems, which means the ship motion and sloshing tank were solved separately, Newman [2005] has analyzed tank/ship motion in WAMIT panel, solved ship motion and tank sloshing in a unified approach. The approach included the interior wetted surfaces of the tanks as an extension of the conventional computational domain which was defined by the exterior wetted surface of the body.

However, the methods used above were all linear, some researchers found it might not reasonable to assume internal liquid sloshing flow in linear potential theory. Kim [2001] and Kim *et al.* [2004] adopted finite-difference method (FEM) to compute slosh-induced forces and moments. Kim [2002] used FEM to simulate a three-dimensional sloshing flow in tanks. A time-domain panel is used to compute ship motion. The forces and moments of sloshing tanks were added on wave-induced excitation, meanwhile, displacement, velocity and acceleration have been applied to the excitation of tank sloshing. Nam *et al.* [2009] also used FEM to simulate the sloshing flows, and compute ship motion in impulsive-response function (IRF). They carried out both numerical and experimental studies of LNG FPSO model and compared their numerical results with those in experiments. In recent decades, many studies used viscous flow theory in order to solve the nonlinearity of the tank sloshing, and with the development of computational technology, more and more researches have been done by computational fluid dynamics. Li *et al.* [2012] and Jiang *et al.* [2015] both applied viscous flow theory under OpenFOAM to compute violent flow in tanks. Nevertheless, the studies both solve ship motion in potential

theory, which ignore the influence of viscous in the external region and the fully coupling of ship motion and sloshing tanks. Shen and Wan [2012] realized the fully coupled methods of ship motion and tank sloshing through the unsteady RANS solver, naoe-FOAM-SJTU. The simulation was done by solving Navier–Stokes equation both in external and internal region. A KVLCC2 model was chosen to compare with experimental results and then the coupling effect was observed in KVLCC2 model coupled with two LNG tanks.

In this paper, a simplified FPSO coupled with LNG tanks is simulated by CFD method. The internal sloshing tank and external sea waves are treated as an entire computational region, and both were solved by RANS solver simultaneously. The Volume of Fluid (VOF) method is applied to capture both outside wave surface and sloshing liquid surface. The forces and moments from both tank sloshing and external wave are integrated together to predict ship motions. The ship motion and tank sloshing are fully coupled. The computations are solved by our in-house URANS solver naoe-FOAM-SJTU, developed based on the open source tool packages, OpenFOAM. The solver contains 6DOF module and dynamic deformation mesh module. The wave generation system uses different methods like piston, flap and boundary inlet to generate first and high order nonlinear waves [Cao *et al.* (2011); Cao and Wan (2012)].

The main objective of the current work is to study the coupling effect of ship motion with sloshing tanks and impact loading. A simplified LNG FPSO is chosen and five different filling ratios of sloshing tanks in regular waves are selected. The ship motion is restricted to three degrees-of-freedom. The results of the simulations are compared with existing experimental results to prove the ability of our solver. Time history of ship motion is carried out and the coupling effect is observed through the ship motion. Considering the influence of wave amplitude, wave frequency and different liquid filling conditions, the coupling effects of ship motion and sloshing phenomenon are analyzed. In particular, ship motion natural frequency and sloshing motion natural frequency are considered. Next, the impact loading on bulkhead is discussed to observe the impulsive phenomenon. Different external wave frequency and amplitude have various influences on the impact pressure.

2. Numerical Methods

Ship coupled with two prismatic tanks is shown in Fig. 1. Two coordinate systems are used to solve ship motion. One system is earth-fixed system ($oxyz$) and the other is body-fixed system ($o'x'y'z'$). To keep the ship body in balance, the body-fixed system is defined at the rotation center of ship model. Both external wave flow and ship motion are solved using the methods described below.

2.1. *Governing equations*

The incompressible Reynolds-Averaged Navier–Stokes equations are adopted in this paper to investigate the viscous flow. Using dynamic deformation mesh, the

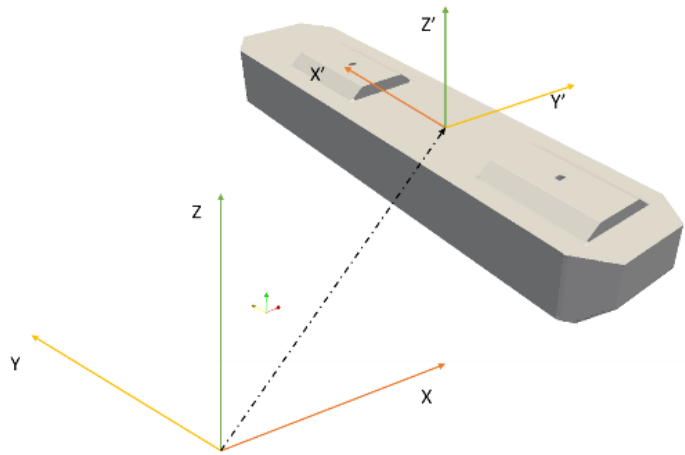

Fig. 1. Description of earth-fixed and body-fixed system.

governing equations are

$$\nabla \cdot \mathbf{U} = 0, \tag{1}$$

$$\frac{\partial \rho \mathbf{U}}{\partial t} + \nabla \cdot (\rho(\mathbf{U} - \mathbf{U}_g)\mathbf{U}) = -\nabla p_d - \mathbf{g} \cdot \mathbf{x} \nabla \rho + \nabla \cdot (\mu_{\text{eff}} \nabla \mathbf{U}) + (\nabla \mathbf{U}) \cdot \nabla \mu_{\text{eff}} + f_\sigma + f_s, \tag{2}$$

where $\mathbf{U}$ is velocity field, $\mathbf{U}_g$ is velocity of grid nodes; $pd = p - \rho \mathbf{g} \cdot \mathbf{x}$ is dynamic pressure; $\mu_{\text{eff}} = \rho(\nu + \nu t)$ is effective dynamic viscosity, in which ν and ν_t are kinematic viscosity and eddy viscosity, respectively. ν_t is obtained by $k - \omega$ SST turbulence model [Dhakal and Walters (2009)]. f_σ is the surface tension term in two phases model. The solution of momentum and continuity equations is implemented by using the pressure-implicit spit operator (PISO) algorithm [Issa (1986)]. PISO algorithm applies mass conservation into pressure equation, thus when pressure equation converges, continuity error decreases. This method uses a predictor–corrector on solving pressure-velocity coupling, and utilizes a collocated grid method [Rhie and Chow (1983)].

2.2. *Volume of fluid method*

The Volume of fluid (VOF) method with bounded compression techniques is applied to control numerical diffusion and capture the two-phase interface efficiently. The VOF transport equation is described below:

$$\frac{\partial \alpha}{\partial t} + \nabla \cdot [(\mathbf{U} - \mathbf{U}_g)\alpha] = 0, \tag{3}$$

where α is volume of fraction, indicating the relative proportion of fluid in each cell and its value is always between zero and one:

$$\begin{cases} \alpha = 0 & \text{air} \\ \alpha = 1 & \text{water} \\ 0 < \alpha < 1 & \text{interface.} \end{cases} \tag{4}$$

To capture the sharp interface and ensure conservation and boundedness, an extra term is added into VOF transport equation:

$$\frac{\partial \alpha}{\partial t} + \nabla \cdot [(\mathbf{U} - \mathbf{U}_g)\alpha] + \nabla \cdot [\mathbf{U}_r(1-\alpha)\alpha] = 0. \tag{5}$$

The added term is nonzero only at interface, thus it doesn't affect solution at another region except interface. $\mathbf{U}_r$ in Eq. (5) is the velocity field used to compress the interface. It is normal to the interface so it does not affect the flow along interface. The description of $\mathbf{U}_r$ is given below:

$$\mathbf{U}_r = n_f \min\left\{ c_\alpha \frac{|\varphi|}{|S_f|},\ \max\left(\frac{|\varphi|}{|S_f|} \right) \right\}, \tag{6}$$

where φ is face volume flux, S_f is normal vector of cell face. The recommended setting of c_α is equal to 1, which maintains the sharp interface.

Besides, the surface tension term in Eq. (2) is defined as

$$f_\sigma = \sigma \kappa \nabla \alpha, \tag{7}$$

where σ is the surface tension coefficient, which is chosen to be $0.07\,\mathrm{kg/s^2}$; κ is the curvature of surface interface, determined by volume of fraction α:

$$\kappa = -\nabla \cdot (\nabla \alpha / |\nabla \alpha|). \tag{8}$$

2.3. *Dynamic deforming mesh*

The ship motion and tank sloshing are solved as a whole, thus only the motion of ship needs the implementation of moving-mesh technique. In this paper, a kind of dynamic deforming mesh is used. The mesh deforms during the computation according to ship motion. The position of the mesh points in the field is solved by a Laplace equation with variable diffusivity:

$$\nabla \cdot (\gamma \nabla x_g) = 0, \tag{9}$$

where x_g is displacement of mesh nodes; γ is diffusivity field, determined by

$$\gamma = \frac{1}{r^2}, \tag{10}$$

where r is distance between cell center to the moving boundary.

2.4. 6*DOF motions*

A fully 6DOF module with bodies is implemented. Two coordinate systems are used to solve 6DOF equation, as mentioned in Fig. 1. We describe $(x_1, x_2) = (x, y, z, \varphi, \theta, \psi)$ as the translation and rotation angles of the ship, representing motions of surge, sway, heave, roll, pitch and yaw, respectively. $(v_1, v_2) = (u, v, w, p, q, r)$ are the velocities in the earth-fixed coordinate system, which can be transformed to the body-fixed coordinate system by equations given below:

$$v_1 = J_1^{-1} \cdot \dot{x}_1 \quad v_2 = J_2^{-1} \cdot \dot{x}_2, \tag{11}$$

where J_1, J_2 are transformation matrices based on Euler angle. The forces and moments are projected into the earth-fixed system in following way:

$$F = (X, Y, Z) = J_1^{-1} \cdot F_e \quad M = (K, M, N) = J_1^{-1} \cdot M_e. \tag{12}$$

The subscript means the forces and moments in the body-fixed system. The linear and angular acceleration in body-fixed system can be described as

$$\begin{aligned}
\dot{u} &= X/m + vr - wq + x_g(q^2 + r^2) - y_g(pq - \dot{r}) - z_g(pr + \dot{q}),\\
\dot{v} &= Y/m + wp - ur + y_g(r^2 + p^2) - z_g(qr - \dot{p}) - x_g(qp + \dot{r}),\\
\dot{w} &= Z/m + uq - vp + z_g(p^2 + q^2) - x_g(rp - \dot{q}) - y_g(rp + \dot{p}),\\
\dot{p} &= \frac{1}{I_x}\{K - (I_z - I_y)qr - m[y_g(\dot{w} - uq + vp) - z_g(\dot{v} - wp + ur)]\},\\
\dot{q} &= \frac{1}{I_y}\{M - (I_x - I_z)rp - m[z_g(\dot{u} - vr + wq) - x_g(\dot{w} - uq + vp)]\},\\
\dot{r} &= \frac{1}{I_z}\{N - (I_y - I_x)pq - m[x_g(\dot{v} - wp + ur) - y_g(\dot{u} - vr + wq)]\},
\end{aligned} \tag{13}$$

where m is the mass of the body; I_x, I_y and I_z are moments of the inertia on the center of rotation; X, Y, Z, K, M and N are surge, sway, heave forces and roll, pitch and yaw moments, respectively; x_{g}, y_{g} and z_g are the vector from the center of gravity to the center of rotation: $(x_{\mathrm{g}}, y_{\mathrm{g}}, z_{\mathrm{g}}) = (x_{\mathrm{cog}}, y_{\mathrm{cog}}, z_{\mathrm{cog}}) = (x_{\mathrm{rot}}, y_{\mathrm{rot}}, z_{\mathrm{rot}})$.

2.5. *Wave generation & damping*

The incoming regular wave is generated by imposing the boundary conditions of α and $\mathbf{U}$ at the inlet. The linear Stokes wave in deep water is applied for the wave generation.

$$\xi(x, t) = a\cos(kx - \omega_e t), \tag{14}$$

$$u(x, y, z, t) = a\omega e^{kz}\cos(kx - \omega_e t), \tag{15}$$

$$w(x, y, z, t) = a\omega e^{kz}\sin(kx - \omega_e t), \tag{16}$$

where ξ is the wave elevation; a is the wave amplitude; k is the wave number; U_0 is the ship velocity; ω is the natural frequency of wave; ω_e is the encounter frequency, in this condition, $\omega_e = \omega$.

3. Validation

3.1. *Geometry and condition*

To validate the current method, a LNG FPSO model with two prismatic tanks is selected. The main particulars of LNG FPSO are shown in Table 1, details can be found in [Nam *et al.* (2009)]. To compare with experiments which have been done by Nam *et al.* [2009], the LNG FPSO model is 1/100 scale of the full scale ship. The length, breadth and height of the fore tank and the aft tank are 49.68 m, 46.92 m, 32.23 m and 56.62 m, 46.92 m, 32.23 m, respectively. The distance from the bottom of tank to the keel line is 3.3 m. The geometry of experimental ship model and numerical ship model is illustrated in Fig. 2. The numerical ship model is a sample filling condition of simplified LNG FPSO.

Table 1. Main particular of LNG FPSO.

Main particulars		Full scale	Model
Scale factor	—	1	1/100
Length between perpendiculars	L_{PP} (m)	285	2.85
Maximum beam of waterline	B_{WL} (m)	63	0.63
Draft	T (m)	13	0.13
Displacement	$\Delta(\mathrm{m}^3)$	220.017.6	220.0176
Natural period of roll	T_ϕ(s)	13	1.3
Vertical center of gravity (from keel)	KG (m)	16.5	0.165
Radius of gyration	K_{xx}	19.45	0.1945
	K_{yy}	71.25	0.7125

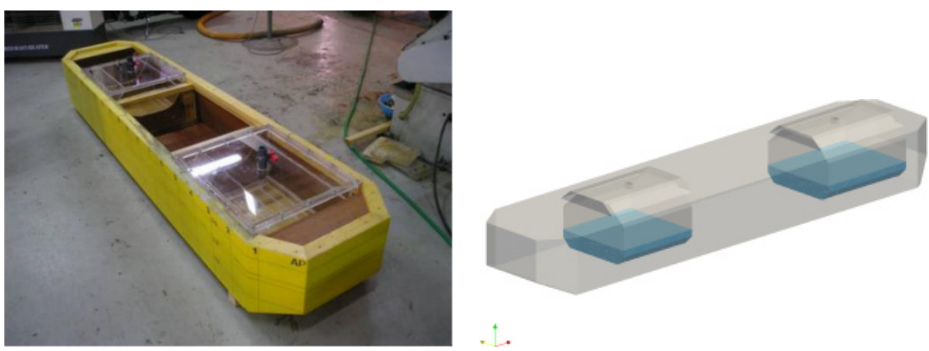

(a) Experimental ship model

(b) Numerical simulation model (30%–30% filling ratio)

Fig. 2. Geometry of LNG FPSO.

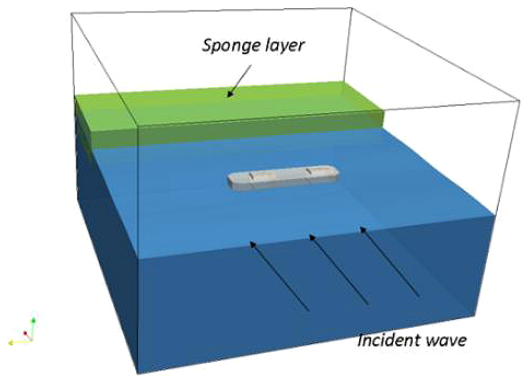

Fig. 3. Setup of numerical computation.

Five different filling conditions are included to verify the computations. The settings of numerical computation are illustrated in Fig. 3, the wave direct is 90°. To ensure the mass conservation of wave generation, a wave sponge layer is set in the computational domain. Compared with experimental data, the filling ratios carried out are the same as those in experiments and the first stands for filling ratio in fore tank, the last stands for filling ratio in aft tank: 0–0% (fore tank-aft tank), 20–20%, 30–30%, 57.5–43.3% and 82.6–23.5%. The daft at each condition was kept the same, as well as longitudinal moment inertia.

Considering the large-amplitude motion of LNG FPSO, the length of regular wave is chosen as 2.865 m, 1.005 times the length of the ship. Same as the experiment, the wave height is fixed as 0.025 m, and encounter frequency as 4.6382.

3.2. *Mesh*

The selected computational domain is described as $-1.0L_{\mathrm{pp}} < x < 2.0L_{\mathrm{pp}}$, $-1.5L_{\mathrm{pp}} < y < 1.5L_{\mathrm{pp}}, -1.0L_{\mathrm{pp}} < z < 1.0L_{\mathrm{pp}}$, the meshes are generated by *snappy HexMesh*, an auto mesh generation utility provided by OpenFOAM. The total cell numbers are around 2.1M, and in order to capture the sloshing phenomenon in tanks, the LNG tanks require additional 0.5M cells. Figure 4(a) illustrates two small tunnels which are used to connect the LNG tanks to the external region. The two tunnels can keep the pressure inside the tanks the same as that in the external region, and simplify the computations. These two tunnels make the external and internal region a whole region, thus the fully coupled effects can be considered. Figures 4(b) and 4(c) show the detail of mesh generation of the bow and stern of the ship.

3.3. *Results*

The ship motion was restricted to three degrees-of-freedom, heave, pitch and roll. Beam wave conditions are analyzed first. The normalized motion amplitude and

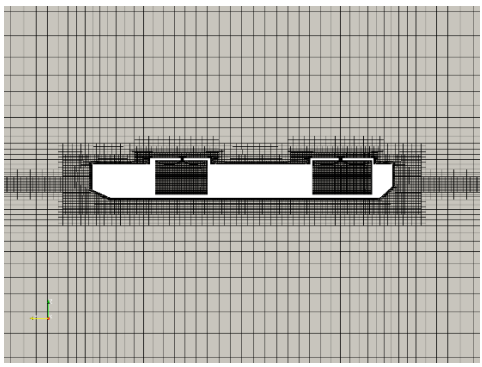

(a) Ship hull with tanks

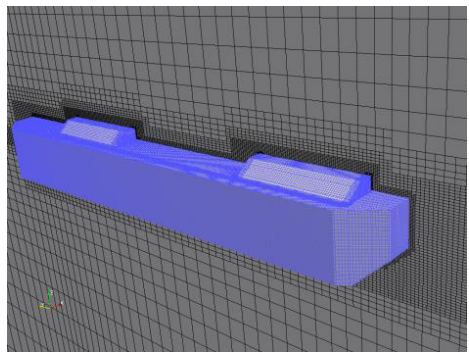

(b) Bow

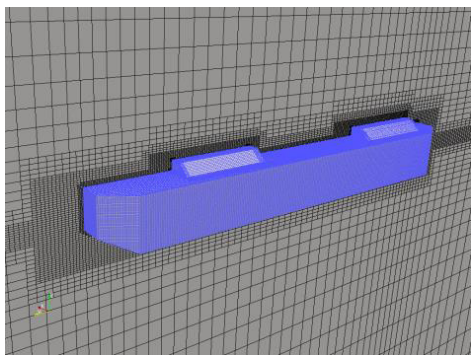

(c) Stern

Fig. 4. Demonstrations of meshes.

natural frequency were considered for comparison with experimental data. The normalized roll motion is given as: $R_1 = \theta B/2A$, in which θ is maximum degree of roll motion, B is beam of ship and A is wave amplitude; The normalized heave motion is given as: $H_1 = \xi/A$, in which ξ is the maximum value of heave motion; and normalized natural frequency is given as: $T = \omega(L/g)^{(1/2)}$, where ω is natural frequency of water, L represents length of ship. When the wave length is close to ship length, $T = 2.5$ s.

Table 2 is the filling condition of present investigation, and Fig. 5 shows the comparison of roll motion between current computation and experiments. Five different filling conditions were considered, and the results fairly agree with those in experiments. We also considered the work of Jiang *et al.* [2015], which solves the same problem using CFD in the inner tank and IRF method in the outer region. It can be seen that the results from Jiang *et al.* [2015] had discrepancy with experimental results, especially under 30–30% and 57.5–43.3% filling conditions. It implies that the viscous in the outer region cannot be ignored. Therefore, the numerical method used in this paper is reliable in solving the current problems.

Table 2. Filling conditions in present investigation.

Case	Filling in fore tank	Filling in aft tank
1	0%	0%
2	20%	20%
3	30%	30%
4	57.5%	43.3%
5	82.6%	23.5%

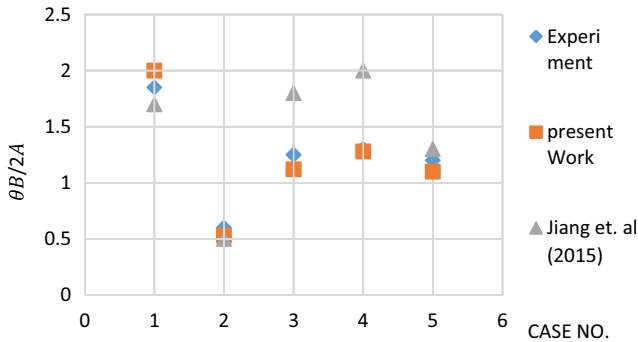

Fig. 5. Comparison results of normalized roll motion with different filling ratios.

4. Coupling Effects on Ship Motion

Numerical simulations of ship motion coupled with partially filled tanks in beam waves are carried out. Figure 6 shows the time history curves of heave and roll motion in different filling ratios. The time history curves indicate that the ship exhibits sinusoidal motion both in heave and roll motion. The coupling effects are not obvious in heave motion, shown in Fig. 6(a), but quite significant in roll motion, shown in Fig. 6(b). Compared to the zero-filling condition, the four partially filling conditions of sloshing tanks all reduce the roll amplitude of ship motion under this wave frequency. The anti-rolling effects are generated by inner sloshing tanks, especially for those in low-filling condition, like 20%–20%, the decrease in amplitude of roll motion is evident and thus shows great coupling effect. For the water in tanks being shallow, the sloshing in tanks is more violent and has more influence on ship motion.

Ordinarily, the low-filling ratio is dominant on coupling effects. In Fig. 6(b), the roll motion amplitude of 82.6%–23.5% filling condition is smaller than that of 57.5%–43.3% filling conditions, which indicates that the low-filling ratio is still dominant in mixed-filling conditions.

Different incident wave frequencies have influence on the coupling effect, especially around ship motion natural frequency or sloshing tank natural frequency. According to ship roll motion RAOs [Jiang *et al.* (2015); Nam *et al.* (2009)], two

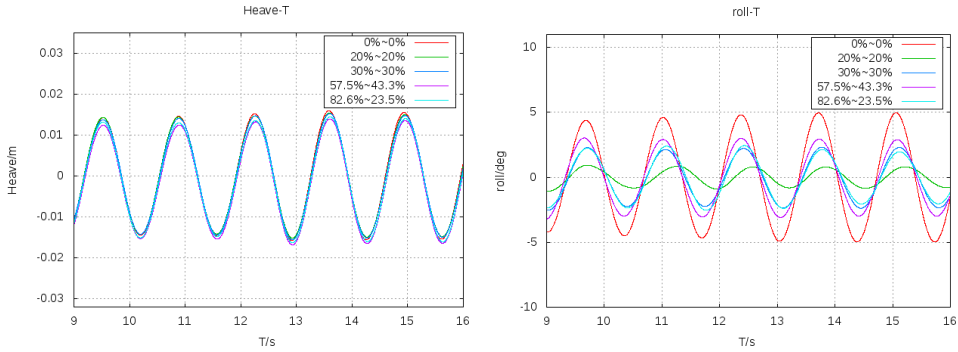

(a) Heave motion (b) Roll motion

Fig. 6. Time history of heave and roll motion with different filling ratios demonstrations of meshes.

different incident wave frequencies are considered. One is equal to ship motion natural frequency ($\omega(L/g)^{1/2} = 2.25$), and the other is equal to the natural frequency of the ship coupled with two sloshing tanks ($\omega(L/g)^{1/2} = 3.5$). To ignore the influence of different filling ratios in aft and fore tank, 30%–30% filling condition is chosen. The wave height is chosen to be 0.1 m, and the time history curves of ship roll motion are shown in Fig. 7. It can be seen that the motion amplitude in Fig. 7(a) is smaller than that in Fig. 7(b), which means the motion response is violent around ship motion natural frequency.

The global view of ship motion and tank sloshing is shown in Fig. 8. It can be observed that in $\omega(L/g)^{1/2} = 2.25$, the crest of the liquid in aft and fore tank reaches the bulkhead at the same time; while in $\omega(L/g)^{1/2} = 3.5$, the crest of liquid in aft tank reaches the bulkhead before that in fore tank. Therefore, the sloshing forces generated by aft and fore sloshing tank are canceled in $\omega(L/g)^{1/2} = 3.5$. The

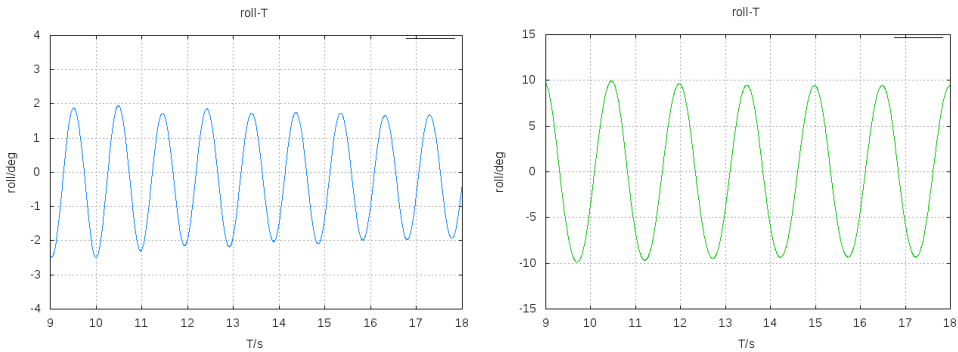

(a) $\omega(L/g)^{1/2} = 3.5$ (b) $\omega(L/g)^{1/2} = 2.25$

Fig. 7. Time history of roll motion in different incident wave frequencies.

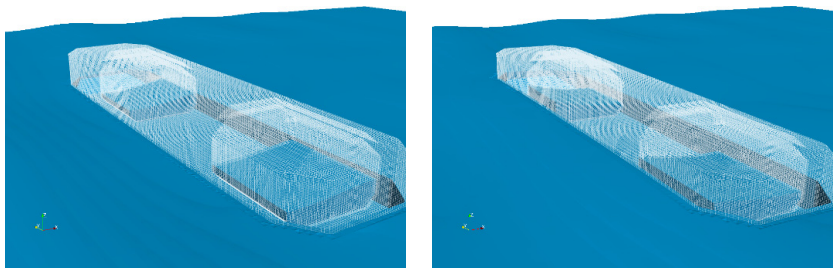

(a) $\omega(L/g)^{1/2} = 3.5$

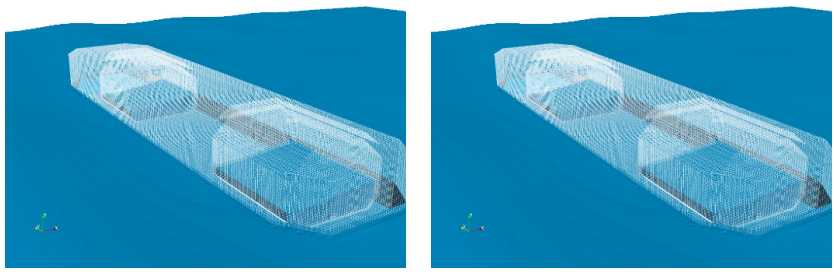

(b) $\omega(L/g)^{1/2} = 2.25$

Fig. 8. Time history of heave and roll motion with different filling ratios demonstrations of meshes.

forces are imposed to the ship motion, thus this phenomenon explains the reason why the roll motion in $\omega(L/g)^{1/2} = 3.5$ is smaller than that in $\omega(L/g)^{1/2} = 2.25$.

The local view of tank sloshing can be seen in Fig. 9. Three snapshots show the wave crest of the liquid in tank, and the wave crest moves from left bulkhead to right bulkhead. It can be observed that when the incident wave frequency is equal to the natural frequency of the object, the sloshing free surface is mild. When the incident wave frequency is equal to the natural frequency of ship motion, the sloshing flow shows a steep run-up. The sloshing liquid climbs the bulkhead when it reaches and an overturning behavior appears.

Considering various kinds of incident wave amplitudes, another wave amplitude is taken into consideration. From roll motion RAOs [Jiang *et al.* (2015); Nam *et al.* (2009)], the ship motion is sensitive to incident wave steepness especially around the ship motion natural frequency. In this paper, we also observed that when the frequency of incident wave is equal to the ship motion frequency, the inner tank sloshing is more violent. Therefore, the incident wave frequency is chosen to be the same with ship motion natural frequency. Figure 10 illustrates time history curves of roll motion under two different incident wave amplitude, and the normalized wave frequency ($\omega(L/g)^{1/2}$) is 2.25. It is obvious that the roll motion is more violent under the larger wave height, for the large wave height brings strong energy. However, when the normalized roll motion is considered, the results show difference. Four

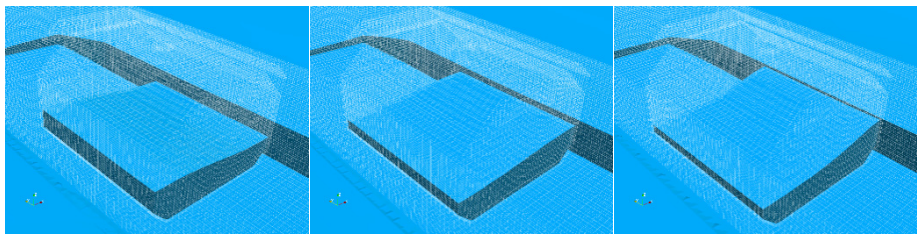

(a) $\omega(L/g)^{1/2} = 3.5$

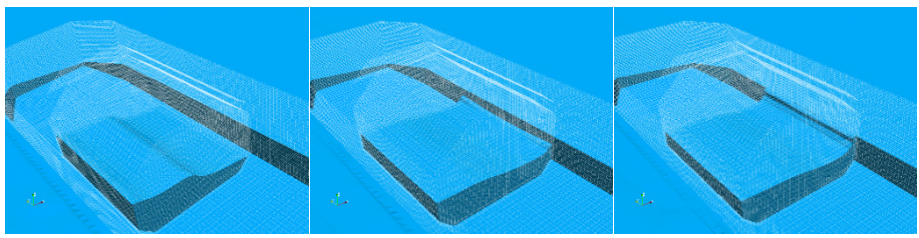

(b) $\omega(L/g)^{1/2} = 2.25$

Fig. 9. Snapshots of LNG FPSO tank sloshing in different incident wave frequencies.

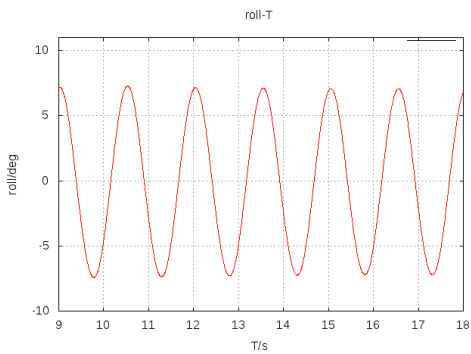

(a) Wave height $H = 0.05\,\text{m}$

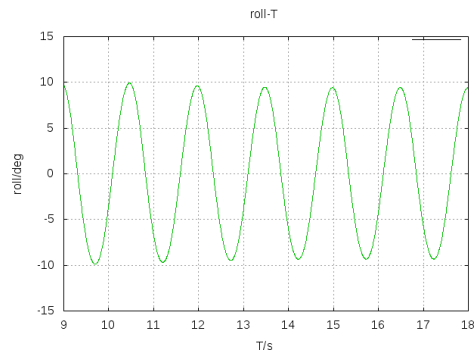

(b) Wave height $H = 0.1\,\text{m}$

Fig. 10. Time history curve of ship roll motion under different wave height.

different cases are listed in Table 3, considering two different wave frequencies and two different wave amplitudes.

As shown in Figs. 9(b) and 11, the comparison of inner tank sloshing under different wave amplitudes shows the influence of sloshing tanks on the roll motion. Snapshots of inner tank sloshing in wave height $H = 0.05\,\text{m}$ are shown in Fig. 11, in which the sloshing surface is not violent like that in Fig. 9(b). The wave crest can be observed in the tank and when it is close to the bulkhead, a run-up also exists. Nevertheless, the overturning phenomenon does not appear, for the incident wave energy is not enough. Thus, the violent tank sloshing in large wave amplitude

Table 3. Environmental settings of four cases.

Case	Incident wave frequency $(\omega(L/g)^{1/2})$	Incident wave height
A	2.25	0.05
B	2.25	0.1
C	3.5	0.05
D	3.5	0.1

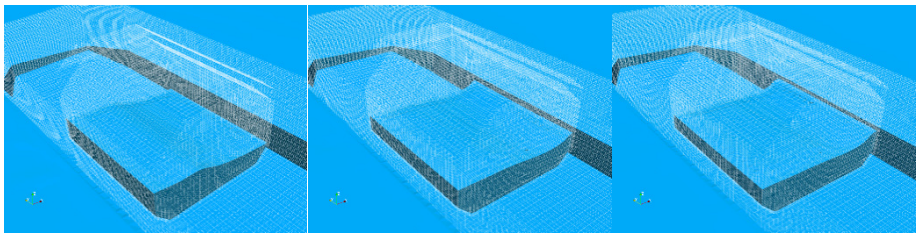

Fig. 11. Snapshots of inner tank sloshing in wave height $H = 0.05\,\text{m}$

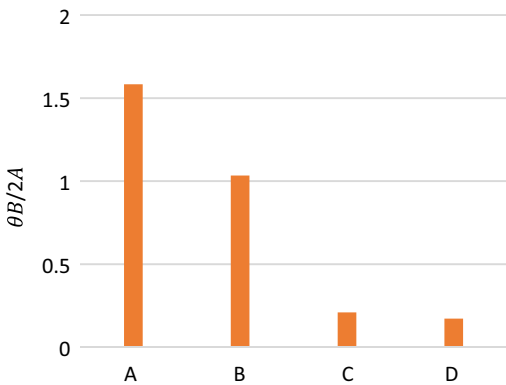

Fig. 12. Normalized roll motion of different incident wave heights and frequencies.

reduces the roll motion much more than that in small wave amplitude. The normalized roll motions of these four cases are shown in Fig. 12. Rather than being large when incident wave height $H = 0.1\,\text{m}$, the normalized roll motion is small in that condition.

The reason is that the forces of sloshing tanks didn't show linear response to the incident wave amplitudes. In the case of $\omega(L/g)^{1/2} = 3.5$, the forces generated from aft and fore tank cancel each other, thus the normalized roll motion did not show much difference in large wave amplitudes.

5. Coupling Effects on Sloshing Impact Pressure

The impact loading on bulkhead of the sloshing tanks is also considered. Figure 14 shows the settings of pressure probes on the bulkhead. The impact pressure is calculated under the condition of 30%–30% filling ratio, two different wave frequencies ($\omega(L/g)^{1/2} = 2.25$ and $\omega(L/g)^{1/2} = 3.5$) and two different wave heights ($H = 0.05\,\text{m}$, $H = 0.1\,\text{m}$) in beam seas. The probe setting is shown in Fig. 13. The pressure probe is situated at still water level in tanks and at first slope corner from tank bottom.

The pressure signals at different sampling points are shown in Fig. 14. Six sampling pressure points are separated into two groups, and it can be seen that the pressure signals in each group are almost identical with each other. None of them shows the impulsive characteristics, which means under this filling condition (30%–30%), the local impact is insignificant when the incident wave frequency is close to ship motion natural frequency or the whole object motion natural frequency.

In Fig. 14(a), two peaks are shown on the pressure curves in the group of $p11$, $p12$ and $p13$, while Figs. 14(b) and 14(c) show only one peak on the pressure curves.

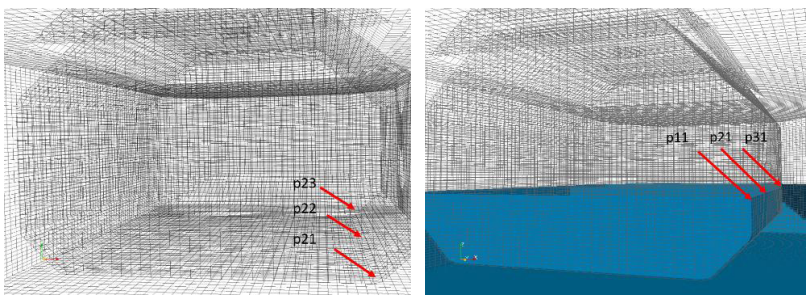

Fig. 13. The settings of pressure probes.

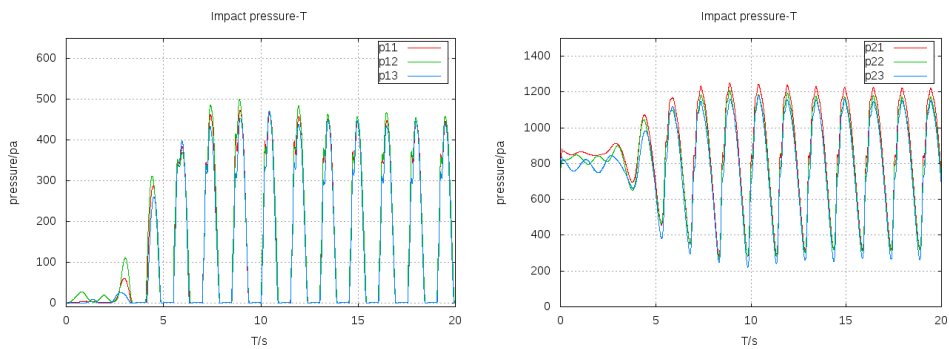

(a) $\omega(L/g)^{1/2} = 2.25;\ H = 0.1\,\text{m}$

Fig. 14. Pressure signals on various probes in different wave frequency and amplitude.

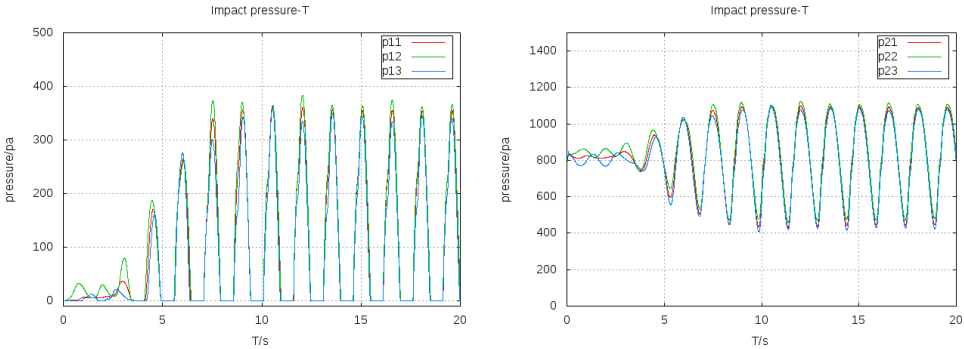

(b) $\omega(L/g)^{1/2} = 2.25;\ H = 0.05\,\mathrm{m}$

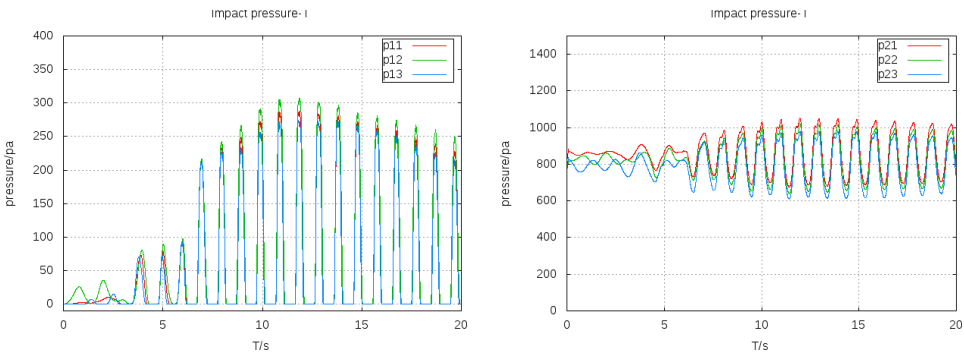

(c) $\omega(L/g)^{1/2} = 3.5;\ H = 0.1\,\mathrm{m}$

Fig. 14. (*Continued*)

Two peaks imply the wave crest in tanks reaches the bulkhead and then turns over and passes the pressure probes again. The overturning behavior is not observed under the situation of wave frequency $\omega(L/g)^{1/2} = 3.5$ and wave height equalling to 0.05 m, thus the pressure curves in these two cases have only one peak. In the group of $p21$, $p22$ and $p23$, the range of pressure amplitude in Fig. 14(a) is wider than that in Figs. 14(b) and 14(c) which means the violent tank sloshing generates large value of pressure amplitude that may cause fatigue damage.

6. Conclusions

In this paper, ship motion fully coupled with internal sloshing tanks and their coupling effects are studied. The numerical simulations are performed by the solver naoe-FOAM-SJTU, which is developed based on open source CFD package OpenFOAM and implemented with dynamic grid technique. The internal tank sloshing and external wave excitation are computed simultaneously by solving RANS equations. Two-phase interface is captured by VOF method. To validate the current method, a simplified LNG FPSO is chosen to compare with existing experimental

data. Five different filling conditions are considered in beam waves. The results show fairly good agreement with those in experiments. In the meantime, the coupling effects are investigated. With the wave length equal to 1.005 times the ship length, the sloshing has little effect on the heave motion. However, the sloshing has remarkable effect on roll motion. The comparison between four different filling ratios with non-filling ratio indicates that all these four kinds of sloshing reduce the roll amplitude of ship motions, especially for those low filling ratios, like 20% filled tanks. Ship motion response is sensitive to incident wave amplitude. For large wave amplitude, the energy makes ship motion response strong but the violent inner tank sloshing reduces the roll motion much more. The cases under different incident wave amplitudes show the nonlinearity of ship motion coupled with sloshing tanks, especially in certain incident wave frequency, where an overturning behavior is observed.

Different incident wave frequencies also influence the ship motion response and tank sloshing. For the incident wave frequency which is close to the natural frequency of ship coupled with partially filled tanks, the global view of ship motion and tank sloshing shows the retardation of wave crest reaching the bulkhead in aft and fore tank. The retardation explains the reduction of ship motion, and thus the tank sloshing is not violent. And for the incident wave frequency which is close to ship motion natural frequency, the ship motion becomes large and sloshing in tanks becomes violent, an overturning behavior is observed. The impact pressure also describes this kind of phenomenon. When the incident wave frequency is close to ship motion natural frequency, the impact pressure at the bottom corner of the tank shows wide pressure amplitude, which can be considered as the structural construct standards.

Acknowledgments

This work is supported by the National Natural Science Foundation of China (Grant Nos. 51490675, 51379125, 11432009, 51579145), Chang Jiang Scholars Program (T2014099), Program for Professor of Special Appointment (Eastern Scholar) at Shanghai Institutions of Higher Learning (2013022), Innovative Special Project of Numerical Tank of Ministry of Industry and Information Technology of China (2016-23/09) and Lloyd's Register Foundation for doctoral students, to which the authors are most grateful.

References

Cao, H. J., Zha, J. J. and Wan, D. C. [2011] "Numerical simulation of wave run-up around a vertical cylinder," In *Proc. 21st Int. Offshore and Polar Engineering Conference* (*ISOPE*) (Maui, Hawaii, USA), pp. 726–733.

Cao, H. J. and Wan, D. C. [2012] "Numerical investigation of extreme wave effects on cylindrical offshore structures," In *Proceedings of the Twenty-Second International Offshore and Polar Engineering Conference* (*ISOPE*) (Rhodes, Greece), pp. 804–811.

Dhakal, T. P. and Walters, D. K. [2009] "Curvature and rotation sensitive variants of the K-Omega SST turbulence model," *ASME 2009 Fluids Engineering Division Summer Meeting*, pp. 2221–2229.

Issa, R. I. [1986] "Solution of the implicitly discretized fluid flow equations by operator-splitting," *J. Comput. Phys.* **62**(1), 40–65.

Jiang, S. C. *et al.* [2015] "Numerical simulation of coupling effect between ship motion and liquid sloshing under wave action," *Ocean Eng.* **108**, 140–154.

Kim, Y. [2001] "Numerical simulation of sloshing flows with impact load," *Appl. Ocean Res.* **23**(1), 53–62.

Kim, Y. [2002] "A numerical study on sloshing flows coupled with ship motion — The anti-rolling tank problem," *J. Ship Res.* **46**(1), 52–62.

Kim, Y., Shin, Y. S. and Lee, K. H. [2004] "Numerical study on slosh-induced impact pressures on three-dimensional prismatic tanks," *Appl. Ocean Res.* **26**(5), 213–226.

Li, Y. L. *et al.* [2012] "Simulation of tank sloshing based on OpenFOAM and coupling with ship motions in time domain," *J. Hydrodyn.* **24**(3), 450–457.

Malenica, S., Zalar, M. and Chen, X. B. [2003] "Dynamic coupling of seakeeping and sloshing," *13th Int. Offshore and Polar Eng. Conf. ISOPE*, Honolulu, HI, May, pp. 25–30.

Mikelis, N. E., Miller, J. K. and Taylor, K. V. [1984] "Sloshing in partially filled liquid tanks and its effect on ship motions: Numerical simulations and experimental verification," *R. Inst. Nav. Archit. Trans.* **126**, 267–281.

Nam, B. W. *et al.* [2009] "Experimental and numerical studies on ship motion responses coupled with sloshing in waves," *J. Ship Res.* **53**(2), 68–82.

Newman, J. N. [2005] "Wave effects on vessels with internal tanks," *Proc. 20th Workshop on Water Waves and Floating Bodies*, Spitsbergen, Norway.

Rhie, C. M. and Chow, W. L. [1983] "Numerical study of the turbulent flow past an airfoil with trailing edge separation," *AIAA J.* **21**(11), 1525–1532.

Rognebakke, O. F. and Faltinsen, O. M. [2003] "Coupling of sloshing and ship motions," *J. Ship Res.* **47**(3), 208–221.

Shen, Z. R. and Wan, D. C. [2012] "Numerical simulations of large-amplitude motions of KVLCC2 with tank liquid sloshing in waves," *Proc. 2nd Int. Conf. Violent Flows, Nantes, France, Ecole Centrale Nantes*, pp. 149–156.